# Separation of Helium-Methane Mixtures by Pressure Swing Adsorption

The separation of mixtures of helium and methane using a single column of activated carbon in a pressure swing adsorption process was studied experimentally. Process performance was predicted with an average error of 10% or less by a local-equilibrium well-stirred cell model in which dead volumes at the feed and product ends of the column were accounted for. Systematic differences between experiment and model were ascribed to omission from the model of flow resistance and heat release.

**H. C. CHENG and F. B. HILL**

Brookhaven National Laboratory
Upton, NY 11973

## SCOPE

Pressure swing adsorption (PSA) processes are widely used industrially for the separation of gas mixtures. The basis of operation of these processes has however not been extensively studied in other than proprietary laboratories. Work from open laboratories which has been published to date has dealt with the separation performance of one- and two-column processes. Process experiments have been performed on nitrogen-methane separation (Turnock, 1968), helium purification (Shendalman and Mitchell, 1972), air separation (Flores, Fernandez, and Kenney 1983), and hydrogen isotope separation (Weaver and Hamrin, 1974; Wong et al., 1980; Wong and Hill, 1982). Comparisons of the data with local equilibrium models have shown that rate processes sometimes limit process performance.

In the work described in the present paper, a high separation factor system—helium-methane-BPL activated carbon—was used to study a simple one-column three-step PSA process. A number of factors not previously examined were varied in the present study: pressure ratio, feed composition, and dead volume. Experimental data were compared to a well-stirred cell local equilibrium process model (Cheng and Hill, 1983) after modification to include dead volume at each end of the adsorption column.

## CONCLUSIONS AND SIGNIFICANCE

Process simulations using the modified well-stirred cell local equilibrium model showed that addition of dead volume to the product end of the column improved separation, whereas addition at the feed end resulted in poorer separation. Product-end dead volume leads effectively to generation of a purge stream in a process otherwise free of a purge step. Feed-end dead volume leads effectively to the introduction of feed with an elevated heavy component content. Depending on their relative sizes, dead volume at both column ends can lead to improved or diminished separation performance.

Experimentally measured helium enrichment in the high pressure product stream qualitatively varied with product cut, pressure ratio, and feed composition in the manner expected for a separation controlled by equilibrium. Furthermore, the use of different rates of pressurization and blowdown and the introduction of delay periods after pressurization and blowdown did not affect helium enrichment in the high pressure product, thus confirming the absence of influence of rate processes.

The well-stirred cell model underpredicted experimental enrichments at small cuts. For the more helium-rich feeds (49.7 and 90% He) this discrepancy decreased as the cut increased, whereas for the most dilute feed (10% He) the model overpredicted the experimental enrichment at large cuts. However, for each continuation of pressure ratio and feed composition the average discrepancy was 10% or less. Arguments are presented which ascribe the discrepancy between model and experiment to omission from the model of flow resistance and heat release.

The results of the work are of value in understanding the basis of operation of PSA processes.

### INTRODUCTION

Pressure swing adsorption (PSA) is a well-established technique for the separation of gaseous mixtures, and is widely practiced industrially. Even though this is true, study of the principles underlying process operation, at least as revealed in the open literature, is in its infancy. Following disclosure by Skarstrom (1959) of Exxon of what is regarded as the first PSA process, the first study of process principles described in the open literature was carried out by Turnock (1968). He studied a two-step one-column process and its performance in separating a nitrogen-methane mixture on a molecular sieve adsorbent. Reasonable agreement was found between experiment and a local equilibrium model (Turnock and Kadlec, 1971). Shendalman and Mitchell (1972) then studied the two-column process of Skarstrom (1959) using helium containing a trace of carbon dioxide with silica gel as the adsorbent. Process start-up transients were compared to the predictions of a local equilibrium model. Solution of the partial differential equation

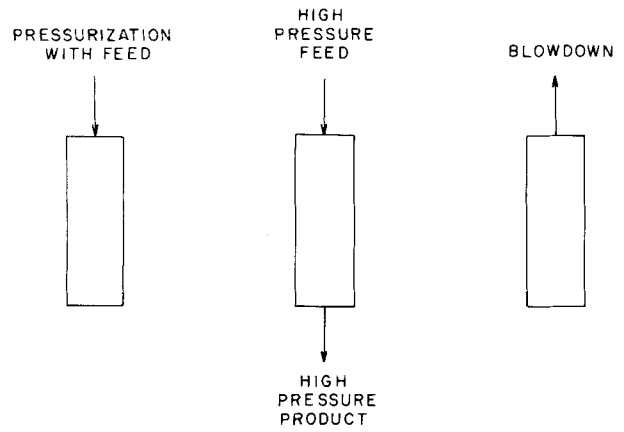


**Figure 1. Steps in single-column PSA process.**

describing the model was by the method of characteristics. A second paper (Mitchell and Shendalman, 1973) attributed discrepancies in agreement between experiment and model to kinetic factors. Air separation was studied by Flores, Fernandez, and Kenney (1983). They used a well-stirred cell local equilibrium model to describe the three-step one-column PSA separation of air on a molecular sieve adsorbent. Good agreement of the model with experiments on this system was found for long cycle times. The separation of hydrogen isotopes has been studied by Weaver and Hamrin (1974), Wong et al. (1980), and Wong and Hill (1982).

Along with these investigations which included both experimental and modeling components, there have been a number of studies concerned exclusively with modeling. All treat PSA in terms of local equilibrium. Chan et al. (1981) completed the analysis of Shendalman and Mitchell (1972) on impurity removal and considered extent of recovery of the light gas. Hill (1980) performed a similar analysis for a one-column process. Nataraj and Wankat (1982) extended the analysis of Chan et al. to multicomponent separations and Knaebel and Hill (1983) extended it to consider binary feed streams of arbitrary composition.

All the studies described in the foregoing paragraph solve the partial differential equations of interest using the method of characteristics and are conceived to construct models in a step-by-step fashion, starting from simple models and adding complexity from step to step. Chihara and Suzuki (1983) took the opposite approach and directly solved by numerical methods the system of partial differential equations applicable for simultaneous consideration not only of equilibrium limits but also of finite rates of approach to equilibrium and of heat release. Although this approach tends to make the perception of effects of each of the several individual phenomena more difficult, it may lead to closer agreement of model and experiment.

Finally, Cheng and Hill (1983) described a well-stirred cell local equilibrium model applicable to any PSA process and illustrated its use for one- and two-column processes.

The present paper describes the results of a phase of an ongoing study of the basis of operation of PSA processes. Specifically it is concerned with one of the simplest of PSA processes, the three-step one-column process, and its performance in separating a mixture with large separation factors, the helium-methane system. The adsorbent was activated carbon. In an experimental study of this system effects of product cut, pressure ratio, and variables affecting kinetic phenomena were determined. Also the important parameter, feed composition, was varied substantially over its complete range. Experimental results were compared with the well-stirred cell model of Cheng and Hill (1983) after modification to include effects of dead volume.

## THEORY

### Process Description

The process modeled is a three-step one-column process (Figure 1) similar to the rapid PSA process of Jones et al. (1980). The cycle for this process consists of pressurization with feed introduced through one end of the column, followed by introduction of additional feed through the same end at high pressure with withdrawal of a product from the opposite end, and ending with blowdown with the exhausted gas leaving via the feed end only. Methane is removed from the $CH_4$-He feed mixture by adsorption on the activated carbon at high pressure during the pressurization step, allowing helium-enriched gas to be withdrawn directly from the column at essentially feed pressure during the constant high pressure feed step. An enriched stream of $CH_4$ is then obtained during a subsequent blowdown step by exhausting the column to a low pressure.

### Cell Model

The adsorption bed is considered to consist of $M$ well-mixed cells, each cell being of length $\Delta z$, as shown in Figure 2. In addition the bed is bracketed by dead volumes at either end consisting of $J$ cells at the feed end and $N$ cells at the product end. These cells contain no adsorbent. Because of interchange between the gas and the adsorbent, the velocity and composition of the gas phase within the bed change with position and time during both the constant-pressure step and steps with changing pressure. Pressure is assumed to vary with time during pressure changes but not spatially. Also, pressure drop due to flow is negligible. The column is assumed to operate isothermally at pressures for which the gas behaves ideally. Furthermore, all dissipative effects, including diffusional resistance and dispersion are neglected and local equilibrium with linear isotherms is assumed throughout the bed. These isotherms are represented by

$$n_l = k_l \frac{P}{RT} y + b_l \tag{1}$$

$$n_h = k_h \frac{P}{RT} (1 - y) + b_h \tag{2}$$

where $y$ is the mole fraction of the less strongly adsorbed or light component, i.e., helium.

With the foregoing assumptions, the three process steps may be described starting with material balances for the light component and for total mass in the adsorption bed and both end volumes. These equations may then be manipulated using the approaches described by Cheng and Hill (1983) to yield the following model equations. (Refer to the footnote regarding the Supplementary Material at the end of the paper.)

For a pressurization step:

$$\frac{dy_{FD_i}}{d\tau} = \left[\frac{J(\alpha_M \gamma_{PD} + 1)}{\gamma_{FD} \alpha_{FD_J}} + J - i + 1\right] (y_{FD_{i-1}} - y_{FD_i}) \tag{3}$$

$$i = 1,2,\ldots,J$$

$$\frac{dy_i}{d\tau} = \frac{M\gamma_{PD}\alpha_M + M - i + 1}{\beta - (\beta - 1)y_{i-1}} y_{i-1} - \left[\frac{M\gamma_{PD}\alpha_M + M - i}{\beta - (\beta - 1)y_i} + 1\right] y_i \tag{4}$$

$$i = 1,2,\ldots,M$$

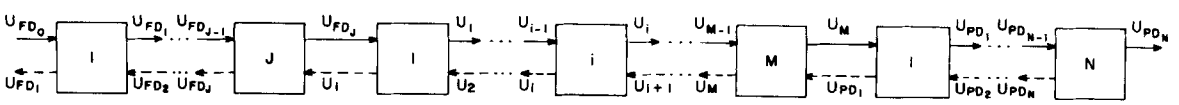


**Figure 2. Flow diagram for cell model.**

and

$$\frac{dy_{PD_i}}{d\tau} = (N - i + 1)(y_{PD_{i-1}} - y_{PD_i}) \qquad (5)$$

$$i = 1,2,\ldots,N$$

where

$$d\tau = \frac{U_0 P_H}{LP[(\alpha_M \gamma_{PD} + 1)/\alpha_{FD_J} + \gamma_{FD}]}\, dt \qquad (6)$$

and $y_{FD_0} = y_F$, $y_0 = y_{FD_J}$, and $y_{PD_0} = y_M$.

For a blowdown step:

$$\frac{dy_{FD_i}}{d\tau} = \left[\frac{J(\alpha_{PD_1}\gamma_{PD} + 1)}{\alpha_1 \gamma_{FD}} + J - i\right](y_{FD_{i+1}} - y_{FD_i}) \qquad (7)$$

$$i = 1,2,\ldots,J$$

$$\frac{dy_i}{d\tau} = \left[\frac{M\alpha_{PD_1}\gamma_{PD} + N - i}{\beta - (\beta - 1)y_{i+1}}\right] y_{i+1} - \left[\frac{M\alpha_{PD_1}\gamma_{PD} + N - i + 1}{\beta - (\beta - 1)y_i} - 1\right] y_i \qquad (8)$$

$$i = 1,2,\ldots,M$$

$$\frac{dy_{PD_i}}{d\tau} = (N - i)(y_{PD_{i+1}} - y_{PD_i}) \qquad (9)$$

$$i = 1,2,\ldots,N-1$$

and

$$\frac{dy_{PD_N}}{d\tau} = 0 \qquad (10)$$

where

$$d\tau = \frac{U_{FD_1}}{(\alpha_{PD_1}\gamma_{PD}/\alpha_1 + \gamma_{FD})L}\, dt \qquad (11)$$

and $y_{FD_{J+1}} = y_1$ and $y_{N+1} = y_{PD_1}$.

For a constant pressure feed step:

$$\frac{dy_{FD_i}}{d\tau} = \frac{J}{\alpha_F \gamma_{FD}}(y_{FD_{i-1}} - y_{FD_i}) \qquad (12)$$

$$i = 1,2,\ldots,J$$

$$\frac{dy_i}{d\tau} = \frac{\beta M}{\beta - 1}\frac{\alpha_{FD_J}}{\alpha_F}\left(\frac{1}{\beta - (\beta - 1)y_{i-1}} - \frac{1}{\beta - (\beta - 1)y_i}\right) \qquad (13)$$

$$i = 1,2,\ldots,M$$

and

$$\frac{dy_{PD_i}}{d\tau} = \frac{N}{\alpha_M \gamma_{PD}}\frac{\alpha_{FD_J}}{\alpha_F}(y_{PD_{i-1}} - y_{PD_i}) \qquad (14)$$

$$i = 1,2,\ldots,N$$

where

$$d\tau = \frac{\alpha_F U_F}{L}\, dt \qquad (15)$$

In these equations

$$\alpha_i = \beta_l[\beta - (\beta - 1)y_i] \qquad (16)$$

$$\beta = \beta_h/\beta_l \qquad (17)$$

$$\beta_h = \frac{\epsilon}{\epsilon + (1 - \epsilon)\rho_p k_h} \qquad (18)$$

$$\beta_l = \frac{\epsilon}{\epsilon + (1 - \epsilon)\rho_p k_l} \qquad (19)$$

$$\gamma_{FD} = V_{FD}/\epsilon AL \qquad (20)$$

$$\gamma_{PD} = V_{PD}/\epsilon AL \qquad (21)$$

One can show that the dimensionless time required for pressurization or blowdown is

$$\tau_P = ln\frac{P_H}{P_L} \qquad (22)$$

Equations 3-5, 7-10, and 12-14 each are a set of $(J + M + N)$ simultaneous first-order differential equations which can be integrated to give the mole fraction profile within the column as a function of the dimensionless time $\tau$ during the step under consideration. The transient profiles for a given PSA cycle are calculated by integrating these sets of equations cyclically in the proper order.

### Process Performance

Two indices of process performance which are of interest are the average steady-state enrichment of the light component in the product stream defined as

$$E = y_{PRD}/y_F \qquad (23)$$

and the steady state recovery of the light component in the product stream

$$\rho = E\theta \qquad (24)$$

where the product cut, $\theta$, is given by

$$\theta = \frac{N_{PRD}}{N_P + N_F} \qquad (25)$$

Since at the cyclic steady state

$$N_P + N_F = N_{PRD} + N_{BD} \qquad (26)$$

Eq. 25 may be expressed as

$$\theta = \frac{N_{PRD}}{N_{PRD} + N_{BD}} \qquad (27)$$

The product mole fraction, $y_{PRD}$, in Eq. 23 is the average steady-state mole fraction leaving the column during the feed step, i.e.,

$$y_{PRD} = \frac{\int_0^{\tau_F} \frac{\alpha_{FD_J}}{\alpha_F}\frac{y_{PD_N}}{\beta - (\beta - 1)y_M}\, d\tau}{\int_0^{\tau_F} \frac{\alpha_{FD_J}}{\alpha_F}\frac{1}{\beta - (\beta - 1)y_M}\, d\tau} \qquad (28)$$

It can be shown that $N_{PRD}$, the moles of gas taken off as product at cyclic steady state during the feed step, is

$$N_{PRD} = \frac{\epsilon AL}{\beta_l}\frac{P_H}{RT}\int_0^{\tau_F} \frac{\alpha_{FD_J}/\alpha_F}{\beta - (\beta - 1)y_M}\, d\tau \qquad (29)$$

Also $N_{BD}$, the moles of gas taken from the column during the blowdown step at the cyclic steady state, is

$$N_{BD} = \epsilon AL\frac{P_H}{RT}\int_0^{\tau_P} e^{-\tau}\left(\frac{\alpha_{PD_1}(\tau)\gamma_{PD} + 1}{\alpha_1(\tau)} + \gamma_{FD}\right) d\tau \qquad (30)$$

### Method of Solution

Mole fraction profiles within the column are calculated by integrating Eqs. 3-5 from $\tau = 0$ to $\tau = \tau_P$ for the pressurization step. An experimentally significant initial condition is $y_{FD_i}(0) = y_i(0) = y_{PD_i}(0) = y_F$. The profile resulting from the integration of Eqs. 3-5 to time $\tau_P$ then becomes the initial condition for the integration of Eqs. 12-14 from $\tau = 0$ to $\tau = \tau_F$ for the feed step. The profiles for $\tau = \tau_F$ then become the initial condition for the integration of Eqs. 7-10 from $\tau = 0$ to $\tau = \tau_P$ for the blowdown step. The cyclic integration of these system equations is then continued until the cyclic steady state is reached.

The GEAR package (Hindmarsh, 1974) was used for the integration. A number of trial integrations were made in which $M$ was varied from 20 to 200. No significant change in $E$ occurred for $M \geq 50$. Hence $n$ was set equal to 50 for all calculations. $J$ and $N$ can be 0 when there is no dead volume, or 1 when perfect mixing occurs in the dead volumes, or any number (15 in these calculations) for different states of mixing in the dead volumes. Dimensionless pa-

rameters varied were separation factor, $\beta$, pressure ratio, $P_H/P_L$, helium feed mole fraction, $y_F$, and the sizes of the dead volumes, $\gamma_{FD}$ and $\gamma_{PD}$.

In evaluating $\beta$, the cells of the adsorption bed were grouped into five sets which each contained ten consecutive cells. The values of $\beta$ at the 5th, 15th, 25th, 35th, and 45th cell were taken as the value of $\beta$ in all cells of the set. Helium was taken to be inert and $\beta_{He} = 0.598$. The adsorption coefficient $k_{CH_4}$ ($= RT\partial n_{CH_4}/\partial P_{CH_4}$) used to calculate $\beta$ was obtained from the experimentally measured adsorption isotherm (see below) and corresponded to the local partial pressure of methane.

## EXPERIMENTAL

### Apparatus

A schematic diagram of the apparatus is shown in Figure 3. A 0.914 m long × 0.0109 m diameter stainless steel tube was packed with Calgon BPL activated carbon particles with diameters in the range $2.1 \times 10^{-4}$ to $4.2 \times 10^{-4}$ m. Physical properties of this carbon are given in Table 1. Feed gases were helium-methane mixtures custom-mixed by the Matheson Co., Rutherford, NJ, with helium concentrations of 10.0, 49.7, and 90.0%.

Three solenoid valves located at the feed and product ends of the column controlled the flow of feed, product, and exhaust gas. These valves were activated by an automatic timer. The volumes between the solenoid valves and the end of the packed column are referred to as dead volumes. At the top in the feed end the size of the dead volume was 9.2 cm$^3$; at the bottom it was 10.6 cm$^3$. The void volume in the column external to the particles was 36.7 cm$^3$. Dynisco pressure transducers with response times of a few milliseconds were located at each end of the column. Back-pressure regulators at each end maintained the high pressure in the column during the feed step and maintained a desired low pressure as the limiting column pressure at the end of the exhaust step.

Part of the product gas flowed through the sample side of a Gow-Mac thermal conductivity cell to provide continuous product composition determination during the constant pressure feed step. Helium flowed through the reference side. During the pressurization and exhaust steps, helium flowing at the same flow rate as the product in the feed step, was directed through the sample side. Transients in thermal conductivity cell output due to nonsteady flow rates were thereby minimized.

### Procedure

Variables fixed for each experiment were the feed gas pressure, the product flow rate, and the cycle time. The low pressure was fixed at 138 kPa. The cycle time is the sum of the pressurization, feed, and exhaust times. These were individually set using the automatic timer. Needle valves in the feed and exhaust lines permitted pressurizing and exhaust gas flow rate adjustment. These flow rates were set to cause gas flow to occur over substantially all of the pressurization and exhaust times.

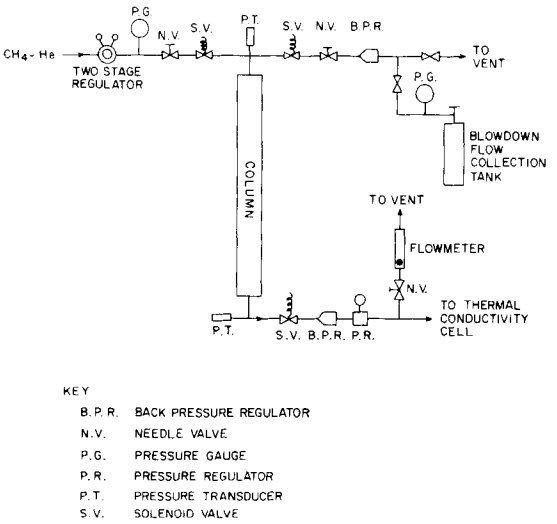


**Figure 3. Schematic diagram of experimental apparatus.**

TABLE 1. PHYSICAL PROPERTIES OF BPL ACTIVATED CARBON

| | |
|---|---|
| Bulk density, $\rho_b$ | 470 kg/m$^3$ |
| Particle density, $\rho_p$ | 850 kg/m$^3$ |
| Real density, $\rho_s$ | 2,100 kg/m$^3$ |
| Intraparticle void fraction | 0.336 m$^3$/m$^3$ bed |
| Interparticle void fraction | 0.43 m$^3$/m$^3$ bed |

In conducting an experiment the column was first equilibrated with the He-$CH_4$ feed mixture at low pressure. Then all solenoid valves were closed. Then after adjusting the feed pressure to the desired pressure, the feed line solenoid valve was opened, initiating the cyclic three-step process. A steady product composition was reached after 10 to 15 cycles. The experiments were conducted at room temperature (298 ± 1 K).

Prior to the experiments the column was evacuated to $10^{-2}$ Pa at 473 K for 5 hours. Heat was provided by means of resistance heating tape wrapped around the column. This procedure was repeated from time to time during the course of experiments.

The product composition and pressure response were measured during the experimental runs. In addition, the product flow rate and exhaust gas flow rate were measured at cyclic steady state. By using various feed times and product flow rates, various product cuts were obtained. The exhaust gas flow rate was found by measuring the pressure increase in the blowdown gas collection tank (Figure 3) for several cycles at the cyclic steady state.

## RESULTS AND DISCUSSION

### Adsorption Isotherm Determinations

The methane adsorption isotherm was measured volumetrically in a separate static system at a temperature of 298 K and pressures up to 1,380 kPa. The data (Figure 4) were fitted to a Langmuir isotherm and could be represented by

$$n_{CH_4} = \frac{1.108 \times 10^{-5} P_{CH_4}}{1 + 1.865 \times 10^{-3} P_{CH_4}}$$

where $n$ is kg-mol of methane adsorbed per kg of carbon at the pressure $P_{CH_4}$ in kPa and 298 K.

From this isotherm it can be shown that $\beta$ ranged from 0.08 to 0.23 for pressures from 138 to 552 kPa for a 10% helium feed. Since as a first approximation the separation factor is $1/\beta$, the corresponding range of separation factors is 12.5 to 4.4.

### Modeling

Effects of dead volumes on process performance were examined through solution of the model equations for various circumstances.

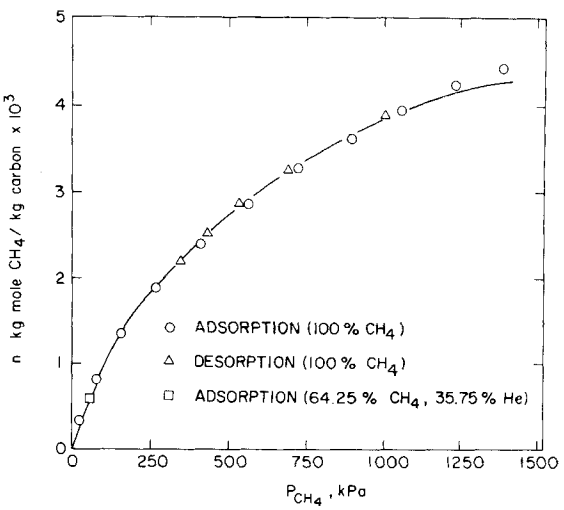


**Figure 4. Methane adsorption isotherm on Calgon BPL activated carbon at 298 K.**

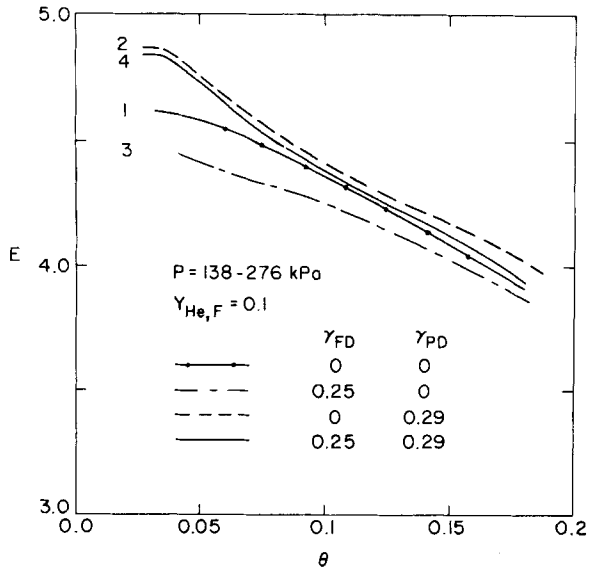


**Figure 5. Effect of dead volume on helium enrichment, $y_F = 0.1$, $P = 138$–$276$ kPa, $\gamma_{FD} = 0.25$ and $\gamma_{PD} = 0.29$.**

The equations were solved for a column without any dead volumes and for columns with dead volume on the feed end only, on the product end only, and on both ends. Also, mixing state in the dead volumes was varied. The results are shown in Figures 5–8 in terms of enrichment-cut relations and in Figures 6–8 in terms as well of recovery-cut relations.

Figure 5 is for a feed containing 10% helium with high and low pressures of 276 and 138 kPa. Also, for this figure there was perfect mixing in the dead volumes ($J = N = 1$). Curve 1 in this figure is typical for a one-column process without dead volume (Hill, 1980; Cheng and Hill, 1983). A plateau is found at small cuts. At large cuts the enrichment decreases with cut to a limiting value of unity. Curve 2 is for the same column with dead volume at the product end only. This dead volume is equal to 29% of the column external void volume, as was the case experimentally. Product-end dead volume is seen to improve the separation. It does so by generating a gas in the dead volume enriched in the light component to purge the column during blowdown. Curve 3 is for a column with feed-end dead volume only. As in the experiments, this dead volume was 25% of the column external void volume. Introduction of dead volume at the feed end leads to a decrease in separation performance. This occurs because methane-rich gas from the exhaust step is left in the dead volume at the end of that step. This gas is richer in methane than the feed. It becomes the first feed gas to be treated in the following pressurization step. Thus with feed-end dead volume the process must actually separate a mixture with a higher average heavy component content than that of the feed. Curve 4 is for the experimental column with dead volume at each end. The result of dead volume at both ends is intermediate between the two extremes and in this case yields performance superior to the absence of dead volume.

In Figures 6–8 the curves shown are the model predictions for the conditions used experimentally. Each figure is for a different

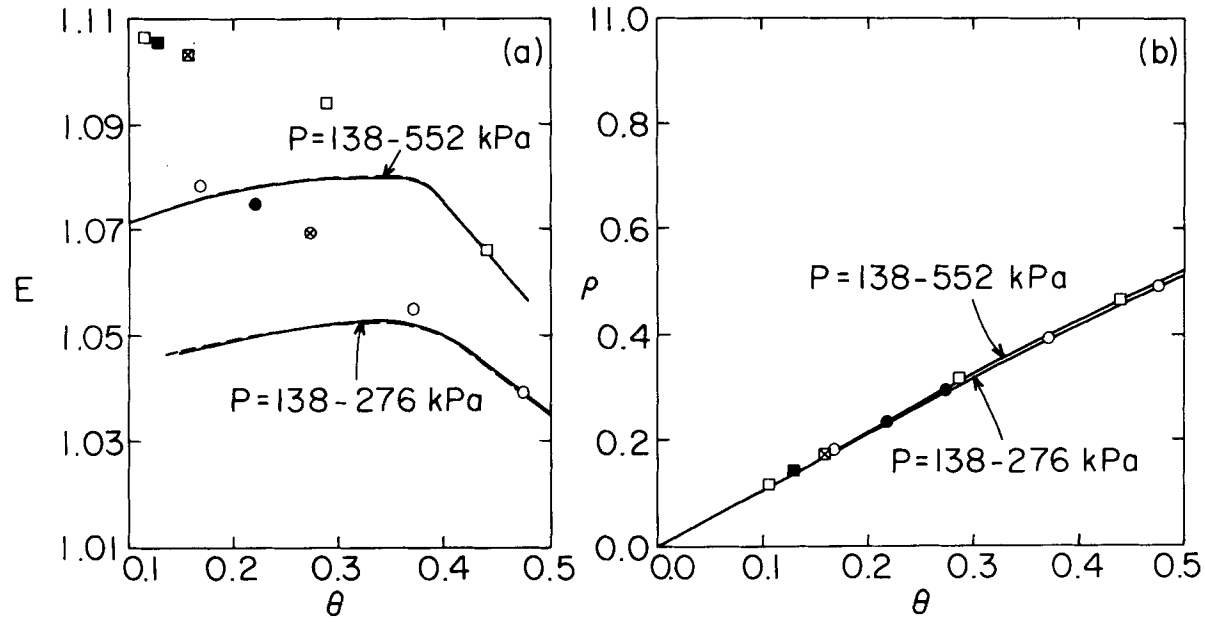


**Figure 6. Helium enrichment and recovery in product as a function of product cut, $y_F = 0.9$.**

***Experimental Data***

| | P (kPa) | $t_p$ (s) | $t_B$ (s) |
|---|---|---|---|
| ○ | 138-276 | 15 | 15 |
| ⊗ | 138-276 | 25 | 25 |
| ● | 138-276 | 15 | 15 with 5 s delay after $t_p$ and $t_B$ |
| □ | 138-552 | 18 | 18 |
| ⊠ | 138-552 | 25 | 25 |
| ■ | 138-552 | 18 | 18 with 7 s delay after $t_p$ and $t_B$ |

***Theoretical Results***

| | J | M | N |
|---|---|---|---|
| --- | 1 | 50 | 1 |
| — | 15 | 50 | 15 |

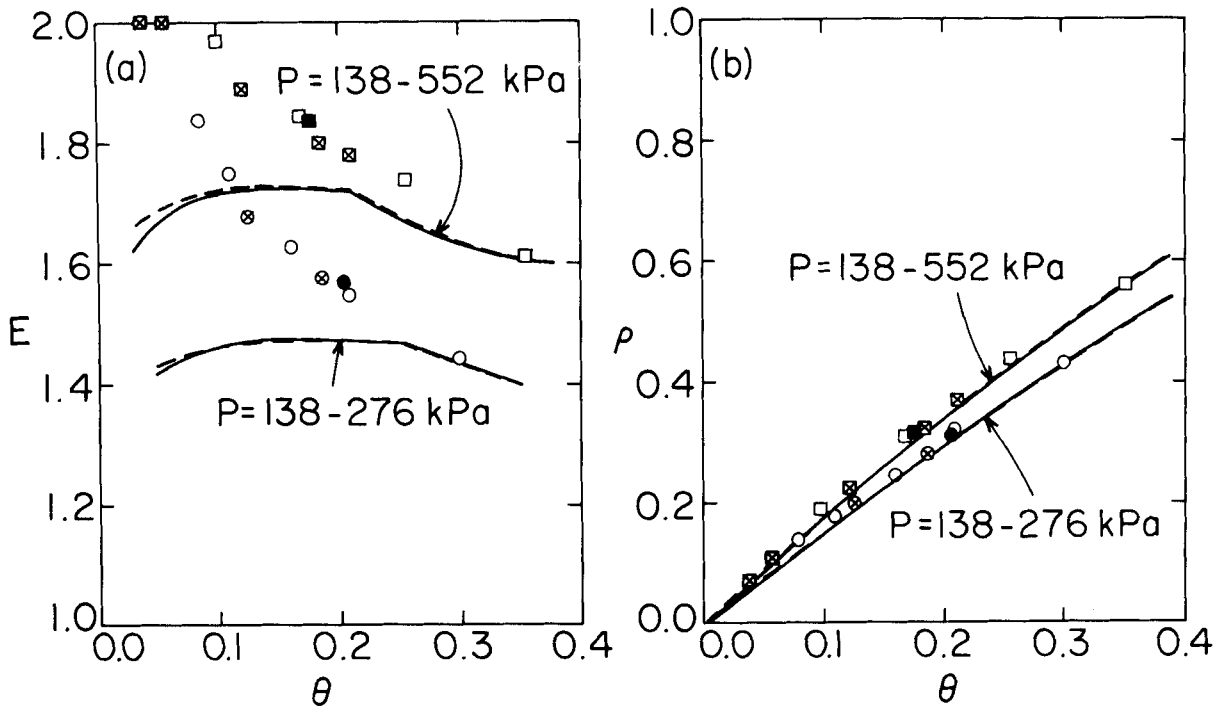


**Figure 7. Helium enrichment and recovery in product as a function of product cut, $y_F = 0.497$.**

***Experimental Data***

| | P (kPa) | $t_p$ (s) | $t_B$ (s) |
|---|---|---|---|
| ○ | 138-276 | 15 | 15 |
| ⊗ | 138-276 | 25 | 25 |
| ● | 138-276 | 15 | 15 with 5 s delay after $t_p$ and $t_B$ |
| □ | 138-552 | 18 | 18 |
| ⊠ | 138-552 | 25 | 25 |
| ■ | 138-552 | 18 | 18 with 7 s delay after $t_p$ and $t_B$ |

***Theoretical Results***

| | J | M | N |
|---|---|---|---|
| - - - | 1 | 50 | 1 |
| — | 15 | 50 | 15 |

feed composition, and shows results for two high pressures, 276 and 552 kPa. Two results are shown for each combination of feed composition and high pressure. The dashed curves are for perfectly mixed dead volumes ($J = N = 1$), whereas for the solid curves the dead volumes were each considered to consist of 15 well-stirred cells ($J = N = 15$). Mixing state is seen to have little effect except for feeds dilute in helium at the high pressure (Figure 8). There increased mixing leads to noticeably better separation.

### Process Experiments

Experimental data are shown for steady state helium enrichment and recovery in Figures 6–8. Data points represented by circles refer to experiments with a high pressure of 276 kPa. Points represented by squares correspond to a high pressure of 552 kPa. As the keys to the figures indicate, differentiation is made for experiments with different rates of pressurization and blowdown and for experiments in which delay periods were introduced following pressurization and blowdown. Cycle times ranged from 45 to 150 s. The ranges of flow step times and flow rates used during the flow step were 15 to 95 s and $0.8 \times 10^{-6}$ to $5 \times 10^{-6}$ std. $m^3/s$, respectively.

Each of Figures 6–8 shows that enrichment decreases with product cut and increases with pressure ratio in qualitative agreement with notions expressed earlier (Hill, 1980; Cheng and Hill, 1983) about spatial fractionation resulting from pressure changes. Thus during pressurization, the light component, because of its higher migration velocity, accumulates preferentially in the closed or product end of the adsorption bed. Then, with a light component mole fraction profile which decreases monotonically from the product end to the feed end, an enrichment which decreases with cut is found. Figures 6–8 also show as expected that the experimental helium recoveries increase with cut.

No significant effects in the data resulted from using different pressurization and blowdown rates or from introducing delay periods following pressurization and blowdown. These results indicate that adsorption and/or desorption rates were not limiting and that local interphase equilibrium determined process performance.

In terms of helium enrichment, the well-stirred cell model generally predicted poorer separation performance than was found experimentally for the feeds rich in helium ($y_F = 0.497, 0.9$). But even so, model predictions were low on the average by only 1 to 10% for different feed mole fraction and high pressure combinations. Helium recovery which is proportional to enrichment necessarily exhibited the same discrepancies between model and experiment. In the most dilute feed ($y_F = 0.1$) the model overpredicted separation performance on the average by 4% (276 kPa) to 10% (552 kPa).

Two causes are suggested to account for the discrepancies observed and these are being investigated further. Both are concerned with an approximation made in model formulation. First, the flow resistance of the bed was assumed to be negligible and thus pressure

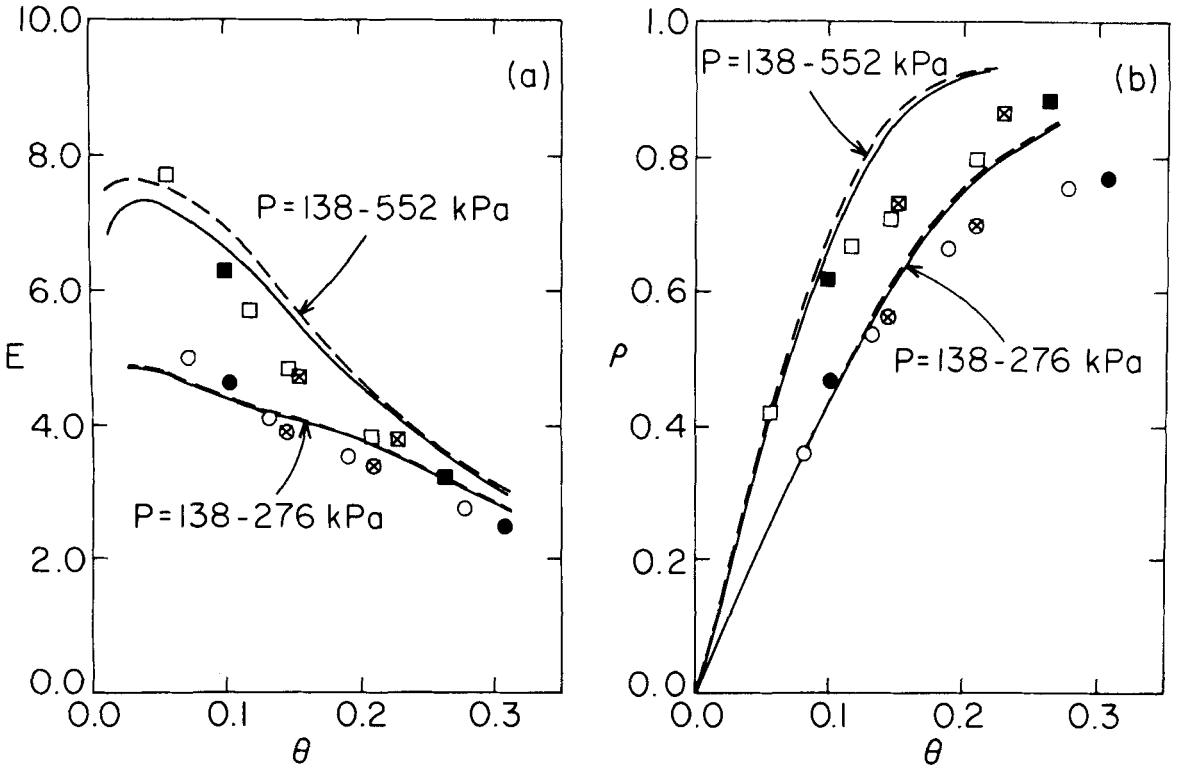


**Figure 8. Helium enrichment and recovery in product as a function of product cut, $y_F = 0.1$.**

***Experimental Data***

| | P (kPa) | $t_p$ (s) | $t_B$ (s) |
|---|---|---|---|
| ○ | 138-276 | 20 | 20 |
| ⊗ | 138-276 | 30 | 30 |
| ● | 138-276 | 20 | 20 with 10 s delay after $t_p$ and $t_B$ |
| □ | 138-552 | 25 | 25 |
| ⊠ | 138-552 | 30 | 30 |
| ■ | 138-552 | 30 | 30 with 15 s delay after $t_p$ and $t_B$ |

***Theoretical Results***

| | J | M | N |
|---|---|---|---|
| --- | 1 | 50 | 1 |
| — | 15 | 50 | 15 |

gradients were assumed absent. That is a good assumption for the constant pressure feed step, for only small differences (7 kPa) were observed between pressures upsteam and downstream of the bed during that step. During pressure changing steps, however, significant pressure differences, up to the difference between the high and low pressures, were noted.

In the absence of pressure gradients, compression or expansion occurs in all parts of the bed simultaneously whereas in the presence of pressure gradients these phenomena are more or less confined to a moving compression or expansion wave. In both cases instantaneous equilibration of adjacent quantities of gas and adsorbent occurs during the compression or expansion step. It seems conceivable that different axial concentration profiles may result in these two instances. Different concentration profiles would lead in turn to different enrichment-cut relations. One type of mole fraction profile which could lead to the discrepancies observed is one which, relative to the profile found in the absence of pressure gradients, exhibits higher mole fractions in the product end of the column and lower mole fractions in the feed end. Relative to the enrichment-cut relation found in the absence of pressure gradients, this type of profile would yield higher enrichment at small cuts but more nearly the same enrichments at large cuts, as found experimentally for the feed mole fractions, $y_F = 0.90$ (Figure 6) and $y_F = 0.497$ (Figure 7). The following argument can be made which supports obtaining the required distortion of the normally expected profile to achieve this result. In the presence of pressure gradients and during a pressurization step, the gas in the compression wave contacts the entire bed in a continuous motion from bed entrance to the closed product end. In so doing, its $CH_4$ content is more completely adsorbed than if the same gas were distributed over the entire length of bed, as it would be in the absence of pressure gradients. Similar reasoning applies to the release of $CH_4$ during a blowdown. Thus local desorption over the entire pressure range is more effective than desorption with the same quantity of gas distributed over the entire bed.

It may be noted that flow resistance was incorporated into the model of Turnock and Kadlec (1971) and that for the longer cycle times used by them these authors found good agreement between their experimental data and model predictions. Computations without flow resistance were not presented by Turnock and Kadlec however. Hence the necessity for including flow resistance has not been established.

The discrepancies between experimental data and model predictions for the most dilute feed ($y_F = 0.1$, Figure 8) require an additional phenomenon as the basis for explanation since the data in this case fall below the model predictions for the most part. Thermal effects are suggested as the cause. These are greatest for this feed, which is 90% methane. Heat released on adsorption raises

the bed temperatuare, reducing the equilibrium capacity for methane so that the spatial fractionation expected during pressurization does not fully occur. This reduced separation is reinforced during blowdown if the heat released during pressurization is not available to assist in the endothermic desorption process. Heat is removed from its release site by conduction and convection during the intervening constant pressure feed step. Heat removal is favored by increasing the duration of the feed step, or, equivalently, the product cut. Thus introduction of heat effects would tend to decrease enrichment and be more effective in this respect as the cut increases. The discrepancies in Figure 8 between experimental data and model predictions thus may be explainable in terms of omission of both pressure gradients and heat release from the well-stirred cell model.


## ACKNOWLEDGEMENT

The authors express appreciation to Randy Meyle for assistance in carrying out the experiments. Activated carbon was supplied by the Calgon Corporation.

This work was supported by the Division of Chemical Sciences, U.S. Department of Energy, Washington, D.C., under Contract No. DE-AC02-76CH00016.


## NOTATION

$A$ = column cross-sectional area
$b$ = intercept in equilibrium isotherm
$E$ = enrichment of light gas in product stream
$i$ = cell number
$J$ = number of cells in feed-end dead volume
$k$ = constant in equilibrium isotherm
$L$ = adsorber length
$M$ = number of cells in adsorber
$n$ = concentration of sorbate in solid phase
$N$ = number of moles entering or leaving adsorber per cycle or number of cells in product-end dead volume
$P$ = gas pressure
$R$ = gas constant
$t$ = time
$T$ = temperature
$U$ = interstitial gas velocity
$V$ = volume of dead volume
$y$ = gas phase mole fraction of light gas
$\Delta z$ = cell length

### Greek Letters

$\alpha$ = defined in Eq. 16
$\beta$ = separation factor $\beta_h/\beta_l$
$\beta_i$ = equilibrium ratio of gas capacity of component $i$ to total capacity of gas and solid phases for component $i$
$\gamma$ = ratio of dead volume to external bed void volume
$\epsilon$ = interparticle void fraction
$\rho$ = recovery of light gas
$\rho_P$ = density of solid particles
$\theta$ = product cut, moles of product per mole of feed
$\tau$ = dimensionless time

### Subscripts

$BD$ = blowdown
$F$ = feed
$FD$ = feed-end dead volume
$h$ = heavy gas
$H$ = high pressure
$l$ = light gas
$L$ = low pressure
$P$ = pressurization
$PD$ = product-end dead volume
$PRD$ = high pressure product

## LITERATURE CITED


Chan, Y. N. I., F. B. Hill, and Y. W. Wong, "Equilibrium Theory of a Pressure Swing Adsorption Process," *Chem. Eng. Sci.*, **36**, 243 (1981).

Cheng, H. C., and F. B. Hill, "Recovery and Purification of Light Gases by Pressure Swing Adsorption," *Industrial Gas Separations*, T. E. Whyte, Jr., C. E. Yon, and E. H. Wagener, Eds., *Amer. Chem. Soc. Symp. Ser.*, **223**, 195 (1983).

Chihara, K., and M. Suzuki, "Simulation of Nonisothermal Pressure Swing Adsorption," *J. Chem. Eng. Japan*, **16**, 53 (1983).

Flores Fernandez, G., and C. W. Kenney, "Modelling of the Pressure Swing Air Separation Process," *Chem. Eng. Sci.*, **38**, 827 (1983).

Hill, F. B., "Recovery of a Weakly Adsorbed Impurity by Pressure Swing Adsorption," *Chem. Eng. Comm.*, **7**, 37 (1980).

Hindmarsh, A. C., "GEAR: Ordinary Differential Equation System Solver," Lawrence Livermore Laboratory Report UCID-30001, Rev. 3, (Dec. 1974).

Jones, R. L., G. E. Keller II, and R. C. Wells, "Rapid Pressure Swing Adsorption Process with High Enrichment Factor," U.S. Patent 4,194,893, March 25, 1980.

Knaebel, K. S., and F. B. Hill, "Analysis of Gas Purification by Heatless Adsorption," submitted to *Chem. Eng. Sci.* (1983).

Mitchell, J. E., and L. H. Shendalman, "Study of Heatless Adsorption in the Model System $CO_2$ in He, II," *AIChE Symp. Ser.*, **69**(134), 25 (1973).

Nataraj, S., and P. C. Wankat, "Multicomponent Pressure Swing Adsorption (MCPSA)," *AIChE Symp. Ser.*, **78**(219), 29 (1982).

Shendalman, L. H., and J. E. Mitchell, "A Study of Heatless Adsorption in the Model System $CO_2$ in He, I," *Chem. Eng. Sci.*, **27**, 1,449 (1972).

Skarstrom, C. W., "Use of Adsorption Phenomena in Automatic Plant-Type Gas Analyzers," *Ann. N.Y. Acad. Sci.*, **72**, 751 (1959).

Turnock, P. H., "The Separation of Nitrogen and Methane by Pulsating Flow Through a Fixed, Molecular Sieve Bed," Ph.D. Thesis, U. of Mich., Ann Arbor (1968).

Turnock, P. H., and R. H. Kadlec, "Separation of Nitrogen and Methane via Periodic Adsorption," *AIChE J.*, **17**, 335 (1971).

Weaver, K., and C. E. Hamrin, Jr., "Separation of Hydrogen Isotopes by Heatless Adsorption," *Chem. Eng. Sci.*, **29**, 1,873 (1974).

Wong, Y. W., F. B. Hill, and Y. N. I. Chan, "Studies of the Separation of Hydrogen Isotopes by a Pressure Swing Adsorption Process," *Sep. Sci. and Tech.*, **15**, 423 (1980).

Wong, Y. W., and F. B. Hill, "Separation of Hydrogen Isotopes via Single Column Pressure Swing Adsorption," *Chem. Eng. Comm.*, **15**, 343 (1982).


*Supplementary material has been deposited as Document No. 04252 with the National Auxiliary Publications Service (NAPS), c/o Microfiche Publications, 214-13 Jamaica Avenue, Queens Village, N.Y. 11428, and may be obtained for $4.00 for microfiche or $7.75 for photocopies.*


*Manuscript received June 21, 1983; revision received October 17, and accepted October 20, 1984.*